Experimental results and first 22Na source image reconstruction by two prototype modules in coincidence of a liquid xenon positron emission tomograph for small animal imaging

M.L. Gallin-Martel, Yannick Grondin, Nicolas Gac, Y. Carcagno, L. Gallin-Martel, D. Grondin, M. Marton, J.F. Muraz, O. Rossetto, F. Vezzu

Experimental results and first ^{22}Na source image reconstruction by two prototype modules in coincidence of a liquid Xenon Positron Emission Tomograph for small animal imaging.

M.-L. Gallin-Martel[a,*], Y. Grondin[b,1], N. Gac[c], Y. Carcagno[a], L. Gallin-Martel[a], D. Grondin[a], M. Marton[a], J.-F Muraz[a], O. Rossetto[a], F. Vezzu[a]

[a] *Laboratoire de Physique Subatomique et de Cosmologie, Université Joseph Fourier Grenoble 1, CNRS/IN2P3, Institut National Polytechnique de Grenoble, 53 avenue des Martyrs, 38026 Grenoble cedex, France*

[b] *Laboratoire TIMC/IMAG, CNRS et Université Joseph Fourier, Pavillon Taillefer, 38706 La Tronche cedex, France*

[c] *Laboratoire L2S, UMR 8506 CNRS – SUPELEC – Univ Paris-Sud, Gif sur Yvette, F-91192, France*

Abstract

A detector with a very specific design using liquid Xenon (LXe) in the scintillation mode is studied for Positron Emission Tomography (PET) of small animals. Two prototype modules equipped with Position Sensitive Photo Multiplier Tubes (PSPMTs) operating in the VUV range (178 nm) and at 165 K were built and studied in coincidence. This paper reports on energy, time and spatial resolution capabilities of this experimental test bench. Furthermore, these experimental results were used to perform the first image reconstruction of a ^{22}Na source placed in the experimental set-up.

Key words : Positron emission tomography (PET), Medical imaging equipment, Liquid Xenon

PACS : 87.57.uk

---

* Corresponding author Tel +33 4 76 28 41 28; Fax : +33 4 76 28 40 04
E-mail adress : mlgallin@lpsc.in2p3.fr (M.-L. Gallin-Martel).
[1] Present address: École Polytechnique Fédérale de Lausanne (EPFL),School of Architecture, Civil and Environmental Engineering (ENAC),Laboratory of Engineering and Environmental Geology (GEOLEP),Station 18,CH-1015 Lausanne,Switzerland

1 Introduction

Small animal imaging aims at observing disease mechanisms or drugs functions. One of the powerful tools used for this purpose is Positron Emission Tomography (PET). Coupled with specific radiotracers injected in the organism, it enables to image molecular biological processes in vivo. One of the challenges of small animal imaging is to obtain high resolution images because of the small dimensions of mouse or rat organ structures. Several PET scanners have been developed in the last decade such as MicroPET II [1] which achieves a resolution less than 0.6 mm RMS. However these PETs are made of several longitudinal slices of radially-oriented crystals. Our detector that is extensively described in [2] uses the scintillation properties of the Liquid Xenon in an axial geometry to provide a three dimensional gamma reconstruction free of parallax error. Several groups are studying using liquid xenon for PET imaging but their approach is slightly different [3,4]. Our detector is sensitive only to the scintillation process and it relies on specular reflections within the light guides.

In [2], only performances of a single LXe prototype module in terms of energy, time and spatial resolution capabilities were estimated. Since then, a new experimental set-up with two LXe modules in coincidence has been built. Present paper deals with its characterization. The first image reconstruction of a ^{22}Na point source located in the centre of the field of view is performed using experimental data sets. The reconstructed image resolutions in the axial, radial and tangential directions are measured. Finally, methods to enhance the image quality are discussed.

2 The experimental set-up for the test of the two modules in coincidence

The experimental set-up used for the test of both prototype modules in coincidence is described on Fig. 1. The Xenon is grade 4.8 (i.e. a purity better than 20 ppm), which is pure enough for our detector concept [2,5]. As in [2], Xenon is liquefied in a compressor then transferred to a container inside the cryostat. The temperature inside the cryostat is kept around 165 K via a liquid nitrogen heat exchanger. The temperature fluctuation is less than a few tenths of a degree. Both Xenon containers (LXe modules) are stainless steel cylinders 50 mm long and 40 mm in diameter, closed at each end with a 3 mm thick suprasil window. Each container can house various types of cells (see Fig. 1). An experimental test bench has been built to allow the x and y measurement and furthermore to evaluate the z-axis localization, the energy and time resolutions.

In [2] the prototype module was equipped with a matrix of 40 UV light guides each featuring a 5 x 2 mm^2 cross-section. In present paper both prototypes modules were equipped with a matrix of 16 UV light guides each featuring a 5 x 5 mm^2 cross-section By doing so, better energy (σ_E/E) and timing (σ_t) resolutions can be achieved but to the detriment of spatial (σ_x, σ_y and σ_z) resolutions.

A ^{22}Na source is mounted on a small carriage moving along the z-axis, in the cryostat. The z-axis of the two LXe modules and the one of the ^{22}Na small carriage are parallels and coplanars. Such an experimental set-up permits us to mimic a 3D image reconstruction of the ^{22}Na source by the 16 modules of a complete μPET LXe detector. It is done by compiling, at first, 8 series of real data acquisitions. Then, this amount of data is treated by an image reconstruction program in which a virtual rotation of both LXe modules is implemented. Finally, it works as if 8 pairs of LXe modules were in coincidence.

The VUV photons are collected with a PSPMT at each LXe module end as in [2]. Hamamatsu provided us with four prototype tubes, belonging to the R8520-06-C12 series [6]. They are

square high resolution position sensitive photomultiplier tubes which are characterized by their compactness and an excellent spatial resolution. Their QE is around 25 % (against 20 % in [2]). These PSPMTs exhibit a 6(X) + 6(Y) cross plate anode. The light pulse position on the photocathode is derived from a barycentre calculation on the X and Y anode signals.

A dedicated read-out electronics was designed to process the PSPMT signals (see Fig. 2). This multi channel module relies on 52 Charge to Digital Converters (QDC) for the charge measurement of anodes and dynodes signals. Each QDC is composed of a gated integrator coupled to a 12 bit Analog to Digital Converter (ADC). The electronics for the experimental trigger comprises two Constant Fraction Discriminators (CFD) and coincidence module (coinc). Each CFD is fed by the analog sum of the dynode signals of the corresponding cell. A Time to Digital Converter (TDC) computes the time difference between the events in the two cells. The coincidence module uses CFD output signal to trigger the QDCs, the TDC and the PC-based data acquisition.

3 Experimental results

3.1 Modules'light guide modelling

It has been demonstrated in the experimental study of a single μPET LXe prototype module [2] that the amount of light collected at a light guide end decays exponentially with the axial z coordinate of the γ photon interaction point. This exponential model is described by :

$$I(z) = I_0 e^{\frac{-z}{\lambda_{ref}}} \qquad (1)$$

The z reconstructed coordinate can be found using the exponential model and the effect of Xenon impurities can be easily introduced in the equations that describe the model [2]. Besides, the main advantage of this model is to qualify the light propagation medium by a single λ_{ref} parameter. The attenuation length λ_{ref} depends on the light guide geometry and its reflectivity.

The number of photoelectrons collected at each module end (module 1 or module 2) is given by:

$$N_{l_{1,2}}(z_{1,2}) = A_{1,2} \cdot \frac{N_{01,2}}{2} \cdot \exp\left(\frac{-l}{\lambda_{ref_{1,2}}}\right) \cdot \exp\left(\frac{-z_{1,2}}{\lambda_{ref_{1,2}}}\right) \qquad (2)$$

$$N_{r_{1,2}}(z_{1,2}) = A_{1,2} \cdot \frac{N_{01,2}}{2} \cdot \exp\left(\frac{-l}{\lambda_{ref_{1,2}}}\right) \cdot \exp\left(\frac{z_{1,2}}{\lambda_{ref_{1,2}}}\right)$$

Where :

- the origin of the $z_{1,2}$ axial coordinates is taken at the centre of each module (1 or 2),
- $A_{1,2}$ is a constant depending on LA and on the PSPMT quantum efficiency for a given module (1 or 2),
- $N_{0_{1,2}}$ is the amount of scintillation photons for a given module (1 or 2),
- l is the module half length.

Unlike in [2], there is no collimation in the z direction so the proposed method for the energy calculation can no longer be used. However, thanks to the exponential model built for the light guide modeling, the reconstructed value of the energy E_{rec} is proportional to $\sqrt{N_r N_l}$:

$$E_{rec} \propto \sqrt{N_r N_l} \qquad (3)$$

Where

- N_r is the number of photoelectrons collected at the right end of a given module,
- N_l is the number of photoelectrons collected at the left end of the same module.

The $\sqrt{N_r N_l}$ distribution for module 1 is given in Fig. 3 for the z_{source}= 0 position. In the present analysis, the axial $z_{1,2}$ reconstruction relies on the dynode signal asymmetry measurement. The photopeak selection in the $\sqrt{N_r N_l}$ distribution obtained for each module permits to level down the background in the $z_{1,2}$ reconstruction.

Finally, the reconstructed axial coordinate z_{rec} of the source position is given by:

$$z_{rec} = \frac{y_{rec1} z_{rec2} - y_{rec2} z_{rec1}}{y_{rec1} - y_{rec2}} \quad (4)$$

where:

- z_{rec1} (respectively $z_{rec2)}$ is the reconstructed axial coordinate of the 511 keV photon emitted by the source in module 1 (respectively in module 2),
- y_{rec1} (respectively y_{rec2}) is the reconstructed transaxial y coordinate (assimilated with the y coordinate of the guide centre) of the 511 keV photon emitted by the source in module 1 (respectively in module 2).

3.2 Calibration

PSPMT and light guides calibration for each module were carried out using Xenon scintillation light as in [2]. The 16 light guides separation is shown on Fig. 4. All of the four guides distributed along the x and y axis can be isolated. As in [2], events reconstructed between two guides are induced by γ-rays undergoing multiple scattering in several guides. Such events can not be processed by PSPMTs. Consequently, a Gaussian fit is performed around each peak in the barycentre distributions illustrated by Fig. 4. Only events within a 1.5 σ range around each peak are used for further analysis. A simulation carried out with the GATE toolkit [2,7-9] shows that the fraction of the events within the 511 keV peak that are cut out is about 50 %. This efficiency loss is due to the localisation method based on

barycentre calculation. A part of these events could be properly processed by a pixelized photodetector [10].

The PSPMTs mapping consists in the determination of a coefficient table that normalizes the right and left responses for each guide when the gamma interaction is located at the module centre.

The light guide attenuation length $\lambda_{ref1,2}$ for each module can be derived from Eq. (5):

$$\ln\left(\frac{N_{r1,2}}{N_{l1,2}} \times C_{1,2}\right) = \frac{2z_{1,2}}{\lambda_{ref_{1,2}}} \quad (5)$$

Where the $C_{1,2}$ coefficient is a measurement of the asymmetry between the left and right end of each guide. The $\lambda_{ref1,2}$ and $C_{1,2}$ coefficient have been calculated using the same calibration method than the one described in [2].The data analysis showed that for each module the 16 λ_{ref} values exhibit a 30 mm mean value and a 1.0 mm standard deviation.

3.3 The axial resolution with the two modules in coincidence

The distribution of the reconstructed z_{rec} position for a source located at $z_{source} = 0$ is shown in Fig. 5. A Gaussian fit of this distribution for various values of z_{source} provides the axial resolution of the two modules experimental set-up. Fig. 6 illustrates the RMS value of the z reconstruction versus the source z position while the Fig. 7 presents the reconstructed position z_{rec} as a function of the source position z_{source}. The average value for σ_{zrec} is around 2.0 ± 0.1 mm.

3.4 The energy resolution and reconstruction with the two modules in coincidence

A Gaussian fit of the photopeak leads (see Fig. 3 for the z_{source}= 0 position) to the σ/μ resolution where σ and μ are respectively the RMS and the mean value of the fitted

distribution. The mean value for the energy resolution is about 10.4 % for the whole module in experimental data analysis (see Fig. 8).

Present results can be compared with values obtained in [11] where both light and charge collection are operated. In [11], detectors use ultra pure xenon, the charge collection makes on line purification necessary on the contrary to our experiment [2]. Moreover in [11], the photodetectors are immersed in the LXe. In these conditions, the energy resolution reached is at the level of 8 % at zero field. Consequently, present results and [11] exhibit a factor of 1.3 in the energy resolution. But it must be stressed that with our concept of detector the z-coordinate determination relies on UV photon absorption [2] inducing a degradation of the energy resolution.

3.5 Time resolution with the two modules in coincidence

The coincidence time resolution has been measured using the TDC signal. Fig. 9 summarizes the coincidence time resolution measurement along the modules by step of 5 mm. A mean value of about 300 ps has been found.

3.6 Summary of the performances and discussion

A two LXe modules in coincidence experimental set-up was built, the optimization of its performances relies on three relevant parameters:

- the axial resolution,
- the energy resolution and reconstruction,
- the time resolution.

In present experiment, a σ_z resolution of 2.0 ± 0.1 mm for a guide to guide coincidence can be reached. Immersing the PSMT in LXe would be the next step towards improving the axial resolution. Actually, the objective consists in optimizing the detector and raising the resolution

at the level of the expected value of 1.5 mm found in [9] where a complete simulation of the detector was done assuming that the PSPMTs were immersed in LXe.

A 10.4 % RMS energy resolution was found in average on the modules' length. In [2], it was demonstrated that the energy calculated using the formula $\sqrt{N_r N_l}$ exhibits a dependence on the z-coordinate, the variation of energy is about 10 % on the whole module. This is a limit of the exponential model. As a consequence, in the present analysis the 10.4 % RMS value found for the energy resolution which relies on the shape of the $\sqrt{N_r N_l}$ distribution is a pessimistic estimation given by the exponential model.

In [12] a time-of-flight positron emission tomography using liquid xenon scintillation is studied. To improve the energy resolution the PSPMT signals have to be corrected according to the location of the interaction point in the detector. The energy resolution after correction is about 11 % RMS. In the present work, our concept of detector favors specular reflections of the UV photons emitted at the interaction point in the light guides and then focus the light onto the PSPMTs. At the difference of [12], the energy resolution is found to be free of the localization of the interaction point no correction is needed. In Fig. 8, the shape of the distribution is rather flat. However, the energy resolution obtained with our detector is very comparable to the [12] corrected one since it is about 11 % RMS. In addition, it should be noticed that in our case the z reconstruction relies on UV photon absorption which degrades the energy resolution.

A 300 ps RMS time resolution in average on the modules' length was measured. It is 1.8 times better than in [2]. But in [2] only a single module was under test and coincidences were made with a LYSO crystal with a poorer resolution. In present experiment, such a resolution has permitted us to level down the random coincidences in the guide to guide experimental data analysis. In [12], the average value of timing resolution is 235 ps RMS. To optimize the time resolution, as to optimize the energy resolution, it is necessary to minimize the amount

of UV photons absorbed before they reach a photo detector. In our case, an improvement in the UV light detection (for example by immersing the PSPMTs in the LXe) improves all the resolutions (σ_E, σ_t and σ_z). Another way to increase the number of photoelectrons is to increase the $\lambda_{ref1,2}$ to minimize the UV photon absoption in the detector. But in this last case, the σ_z resolution will be degraded. Consequently, the optimization of the detector is a matter of compromise.

4 Image reconstruction

4.1 Sampling and image reconstruction

The experimental data were used to quantify the performance of μPET LXe on reconstructed images of ^{22}Na point source located in the centre of the field of view. The image reconstruction of the source located at z = 0 (centre of the modules) was performed with our implementation [13, 14] of the iterative ML-EM algorithm [15]. We first created 2D sinograms by performing a virtual rotation of the projections obtained from the 8 independent runs as explained in section 2. Consequently, a full set of projections is obtained as for a complete scanner. A 2D sinogram is constructed by filling a table with the Radon variables (s,ϕ) identifying the LORs in a transverse plane (see Fig. 10). From the coordinates (x_1,y_1,z_1) and (x_2,y_2,z_2) of the coincident gamma photons in the referential (x,y,z) of the experimental test bench, we determine (s,ϕ) by the following expressions:

$$s = \frac{\det(OP_1, OP_2)}{\| P_1, P_2 \|};\ \cos(\phi) = \frac{(y_1 - y_2)}{\| P_1 P_2 \|};\ \sin(\phi) = \frac{(x_1 - x_2)}{\| P_1 P_2 \|} \qquad (6)$$

where:

- P_1 and P_2 are the geometrical normal projections of the coincident gamma photons on a transverse plane,
- $\det(OP_1, OP_2)$ is the determinant of the two vectors OP_1 and OP2,

- $\|P_1P_2\|$ is the vector P_1P_2 norm.

Each 2D sinogram corresponds to the source projections in a transverse plane identified by the z-coordinate calculated by the equation (4). A sampling path of 1 mm in the z direction has been used to divide the axial field of view in 50 slices, indexed from 1 to 50 in order to have discrete positive values for the image reconstruction step. Hence, a stack of 50 sinograms is obtained. As far as the Radon variables are concerned, a regular sampling that satisfies the Nyquist criteria has been applied. The ϕ variable is sampled according to the total number of light guides composing a module layer in the case of a complete scanner. The number of projections is therefore 64 (16 modules, 4 light guides in a layer). Due to the field of view size, the number of sampled LORs in one projection is a fourth of 64, it means 16 [16]. Therefore in Radon space (s,ϕ), the sinogram is of size 16 x 64 x 50 in s, ϕ and z respectively as shown on Fig. 11. However a common practice in image reconstruction is to interleave the lines of sinograms, which results in dividing by two the number of projections and in doubling the sampling of parallel LORs [16]. The size of the sinogram is therefore 32 x 32 x 50 in s, ϕ and z respectively.

4.2 Axial, radial and tangential resolutions

Fig. 12 and Fig. 13 show the reconstructed image of the source zoomed in axial and transverse views respectively. The axial image horizontal axis corresponds to the z coordinate of the experiment. A linear profile through the point source in this direction shows that the source is well located by the reconstruction process (Fig. 12) at the slices of index 25 and 26. It corresponds to the centre of the module discretized in 50 divisions. With a 1 mm axial voxel dimension, an axial resolution σ_z of 2.20 ± 0.03 mm is calculated.

Fig. 13 shows the radial and tangential linear profiles through the transverse image. With a 2.5 x 2.5 mm^2 transverse voxel dimension, radial and tangential resolutions of 1.27 ± 0.02 mm and 1.13 ± 0.01 mm are calculated respectively.

4.3 Discussion

Several approximations have been made to fill out the sinogram in the Radon space from the coordinates (x_1,y_1,z_1) and (x_2,y_2,z_2) of the two coincident gamma photons. Indeed, our classical implementation of ML-EM algorithm required sinograms in Radon space. It implies (i) interleaving lines of the sinogram, (ii) an arc correction [16], (iii) integration of LORs from several layers into one layer of detectors and (iv) missing data between blocks as illustrated in Fig. 11. The first one is a classical approximation [16], the second and the third approximations correspond to interpolations of the raw data and are therefore quite smooth approximations. The last one is the biggest approximation as illustrated on the sinogram in Fig. 14. Several methods exist to compensate the missing data as exposed in [1] and in [17]. The geometry of the acquisition could be directly modeled in iterative reconstruction methods as it has been done in [1]. It would allow a better quality of reconstruction.

Our acquired data have a quite low signal to noise (only 600 000 events for the image reconstructed). Regularized methods would be therefore appropriate to enhance image quality [18]. The goal of regularization is to add a constraint of smoothness on the reconstructed object in order to be less sensitive to the noise in the data.

The reconstructed image resolutions are at the level of 2.2 mm RMS, 1.3 mm RMS and 1.1 mm RMS respectively in the axial, radial and tangential views. The 2.2 mm axial resolution deduced from the image reconstruction is in nice agreement with the one found thanks to the exponential model and exposed in section 3.3. However, the radial and tangential resolutions are rather optimistic. Indeed, the light guides having a side length of 5 mm, the standard

deviation of a flat distribution is given by $5mm/\sqrt{12} = 1.44$ mm, which is theoretically the best result that it is possible to achieve. This positive bias, which is observed between our measured resolutions and the theoretical limit, is assumed to be caused by the particular position of the source located in the centre of the field of view. It has been reported that spatial resolution measurements should be done with sources off-centred [19], otherwise, the high density of LORs in the centre of the field of view could affect the reconstructed source image intensity. In our case, it has not been possible to test this configuration due to the incomplete modules ring.

The reconstructed image resolution for a MicroPET II according to [20] ranges from 0.35 mm RMS at the centre of the field of view to 0.63 mm RMS in the radial direction, 0.50 mm RMS in the tangential direction and 0.60 mm RMS in the axial direction at 1 cm offset from the centre of the field of view. Improvements are therefore needed to make the μPET LXe more competitive. This should be done mainly by modifying the experimental set-up. Better radial and transaxial resolutions can be achieved by using light guide matrix with a higher number of guides each featuring a smaller cross-section (present one is 5 x 5 mm^2) in the transaxial plane of the camera. A better axial resolution is as well reachable if in the next set-up version the PSPMTs are immersed in the LXe (see section 3.6). These two improvements must be envisaged in the future.

5 Conclusion

Two modules of a parallax error free PET using LXe in an axial geometry have been built. Each module is optically subdivided into 16, 5 x 5 mm^2, MgF_2-coated aluminium UV light guides read on each end by PSPMTs. The light guide modelling has been already extensively discussed in [2]. An experimental test bench has been built. The two modules are read in coincidence to evaluate the axial localization (z coordinate), the energy and time resolutions.

Experimental data have been analyzed using the exponential model. In data analysis, the resolution on the z coordinate has been found to be 2.0 mm once the photopeak is isolated, the energy resolution in average is 10.4 % on the data and time resolution is about 300 ps. The experimental data were used to quantify the performance of PET LXe on the reconstructed image of ^{22}Na point source located in the centre of the field of view. Resolutions of about 2.2 mm RMS, 1.3 mm RMS and 1.1 mm RMS have been found respectively in the axial, radial and transaxial views of the reconstructed image. A complete PET LXe composed of 16 modules was fully simulated in [9], the detector sensitivity was found to be equal to 1 % in the central region in the energy range [250keV, 650 keV].

Improvements are needed to make the μPET LXe more competitive when compared to MicroPET II. The aim of present work was to demonstrate the feasibility of this new concept of axial geometry that would provide a three-dimensional gamma reconstruction free of parallax error. The next step would be now to improve all the resolutions to make possible, with the proposed LXe μPET, to image the distribution of molecular probes at sub-millimetre resolution in laboratory animals. To reach this goal two solutions are to be envisaged simultaneously : using for example 2 x 2 mm^2 light guides matrices [2] in replacement to the present 5 x 5 mm^2 ones to improve the spatial resolutions and immersing the PSPMT in the liquid xenon to improve the energy and time resolutions.

Acknowledgments

Financial support from Institut National de Physique Nucléaire et de Physique des Particules (IN2P3), Région Rhône-Alpes and Université Joseph Fourier is acknowledged. The authors would like to thank Pr. Laurent Desbat from TIMC – IMAG, Techniques de l'Ingénierie Médicale et de la Complexité - Informatique, Mathématiques et Applications de Grenoble - Unité Mixte de Recherche CNRS Université Joseph Fourier UMR 5525, Pr. Michel Desvignes and Dr. Stéphane Mancini from GIPSA-LAB : Grenoble Images Signal Parole et Automatique - Unité Mixte de Recherche CNRS Université Joseph Fourier Université Stendhal - UMR 5216, for their contribution in setting up the image reconstruction software. Dr. Sébastien Jan from SHFJ - Service Hospitalier Frédéric Joliot -CEA Orsay- is thanked for many interesting conversations and bringing his help in using the GATE simulation toolkit. The authors are grateful to André Menthe from the LPSC laboratory for his implication in the technical support of the mechanical part of the experimental test bench. André Braem and his team at CERN are thanked for providing the LPSC laboratory with new samples of MgF_2-coated aluminum leaves used for making the light guides.

References.

[1] Y. Yang *et al*., Phys. Med. Biol NS **49** (2004) 2527.

[2] M-L Gallin-Martel *et al*,Nucl. Instr. and Meth. **A 599** (2009) 275.

[3] M.I.Lopes et al., IEEE Trans. Nucl. Sci. NS-**42**, No6 (1995) 2298.

[4] P. Amaudruz et al. Nucl.Instr. and Meth. **A 607** (2009) 668

[5] J. Seguinot *et al*, Nucl. Instr. and Meth. **A 354** (1995) 280.

[6] Hamamatsu Photonics, 8 Rue du Saule Trapu, Parc du Moulin de Massy, 91300 Massy, France.

[7] S. Jan *et al*., Phys. Med. Biol. **49** (2004) 4543.

[8] S. Jan *et al.*, GATE User's Guide.

[9] S. Jan, PhD Thesis, Université Joseph Fourier (Grenoble, France), Sept. 2002.

[10] A. Braem *et al*., Phys. Med. Biol. **49** (2004) 2547.

[11] K. Ni *et al*, JINST **1** (2006) 9004.

[12] T. Doke *et al*., Nucl. Instr. and Meth. **A 569** (2006) 863.

[13] N. Gac *et al*, EURASIP Journal on Embedded Systems (2008), Article ID 930250.

[14] S. Mancini *et al*, Journal of Real-Time Image Processing (2010), 1.

[15] L.A. Shepp & Y. Vardi. IEEE Trans. Med. Imag. **1** (1982) 113.

[16] D.W. Townsend & B. Bendriem, editors, The theory and practice of a 3D PET (1998) 11.

[17] J.S. Karp *et al*, IEEE Trans. Med. Imag. Vol **7,** No **1** (1988) 21.

[18] R.M. Lewitt and S. Matej, proceedings of the IEEE, Vol **91** (2003), 1588.

[19] M.E Daube-Witherspoon *et al.*, J. Nucl. Med. **43** (2002) 1398.

[20] Y.C. Tai *et al.*, Phys. Med. Biol. **48** (2003) 1519.

List of Figures.

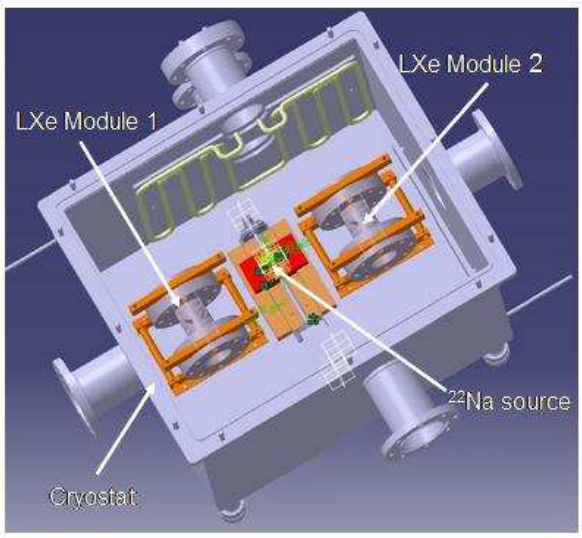

Fig. 1. The experimental set-up used for the test of the two prototype modules in coincidence.

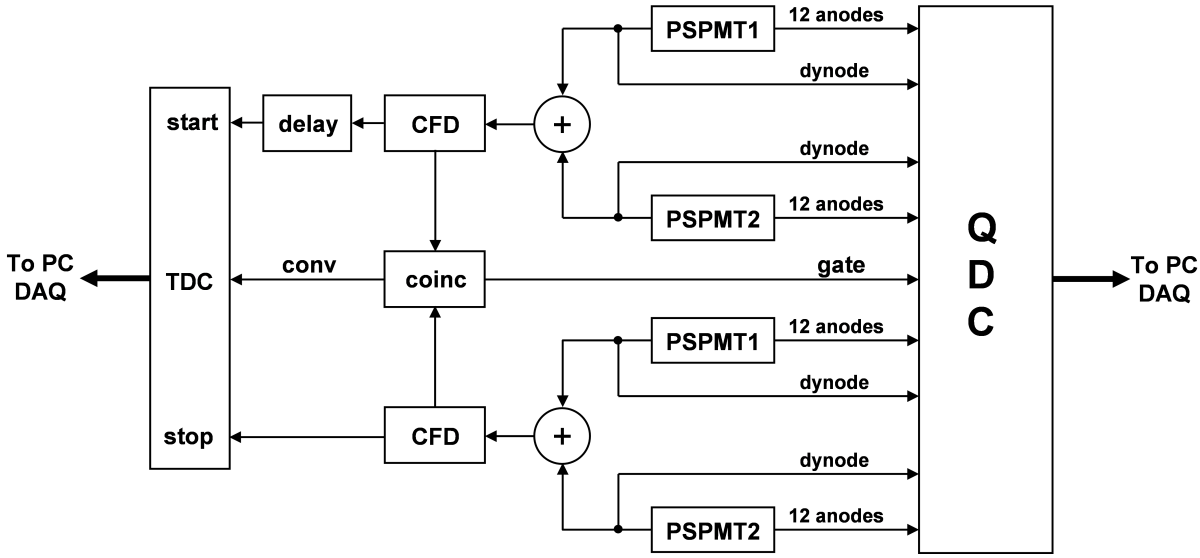

Fig. 2. Data acquisition system.

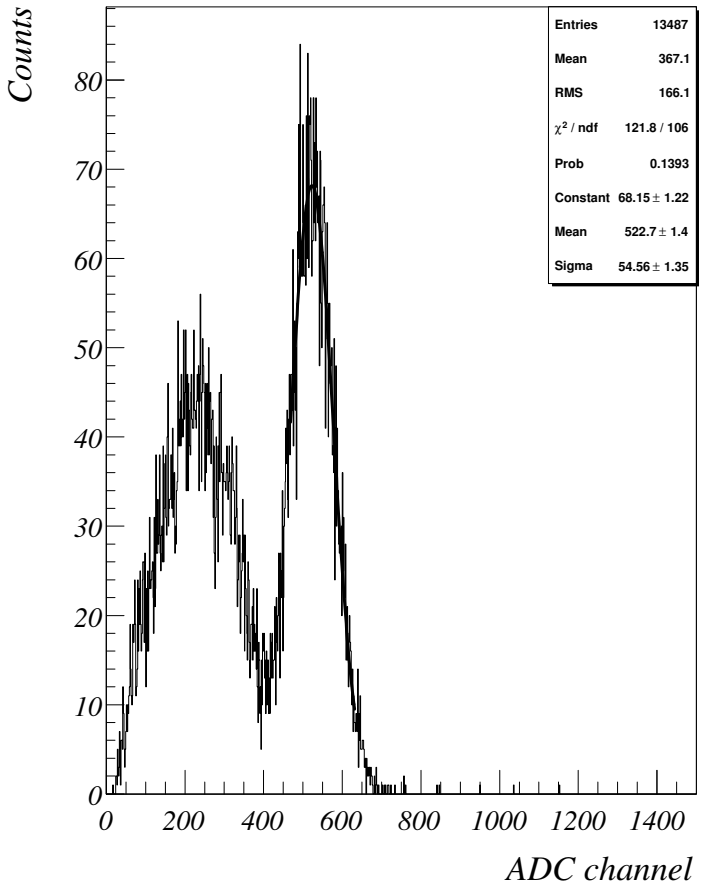

Fig. 3. Spectrum of $\sqrt{N_r N_l}$ obtained for z_{source}= 0 in module 1 – experimental data.

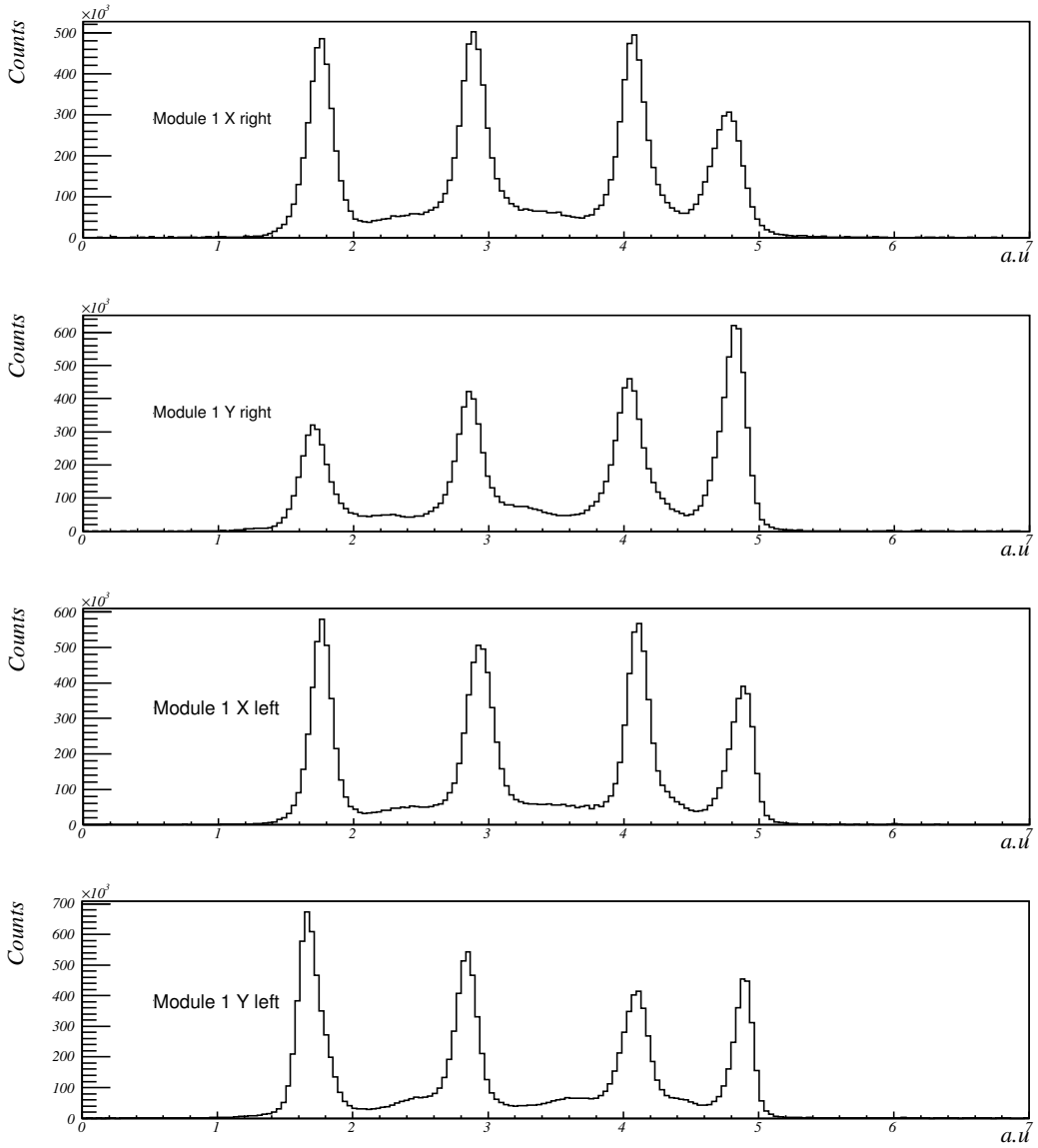

Fig. 4. The x and y barycentre distributions computed by the data acquisition system and derived from the PSPMT anode signals for module 1.

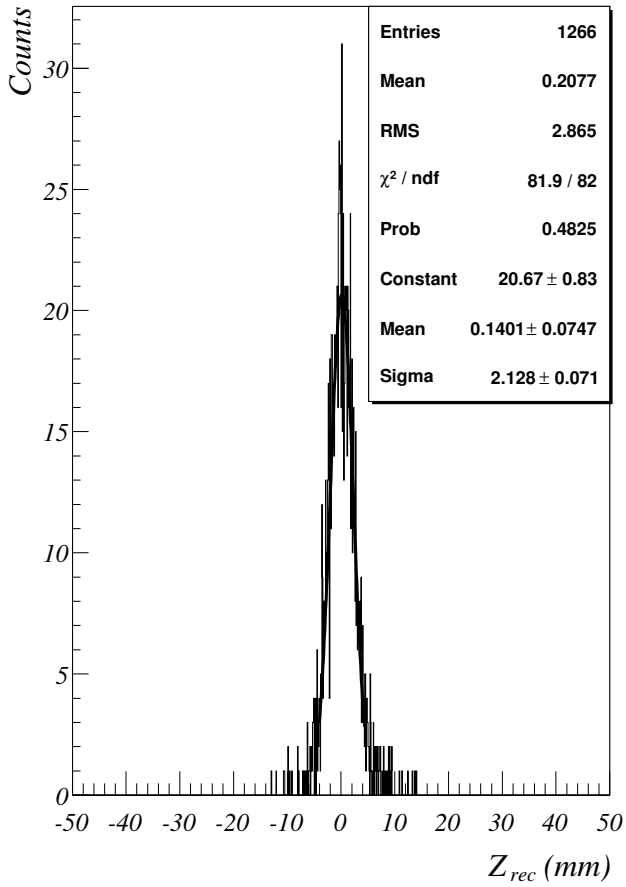

Fig. 5. Distribution of the reconstructed Zrec position for a source located at Zsource = 0 - experimental data.

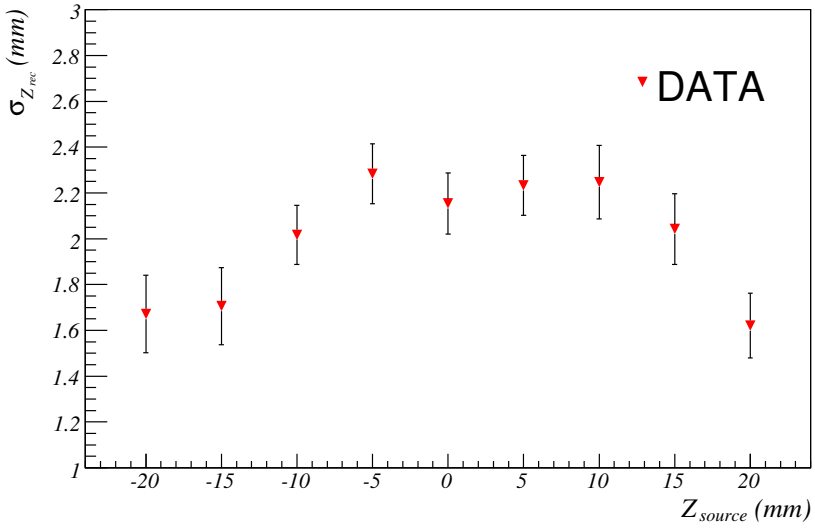

Fig. 6. RMS value of z_{rec} versus z_{source} position.

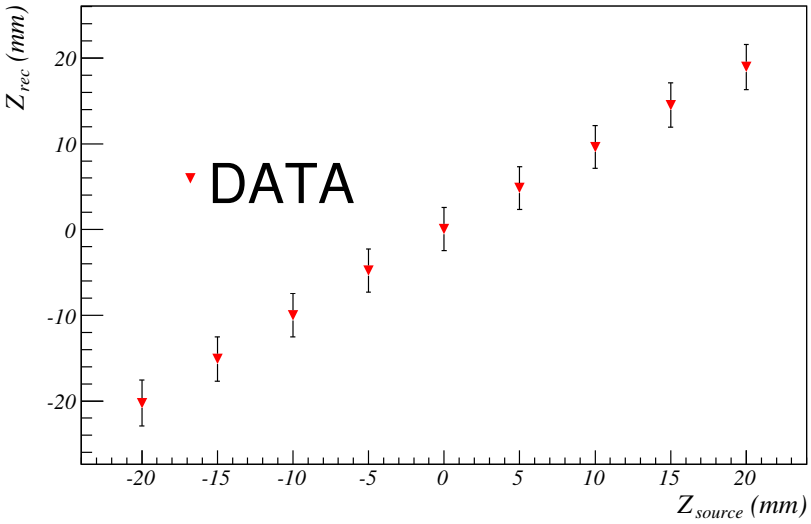

Fig. 7. z_{rec} versus z_{source} position

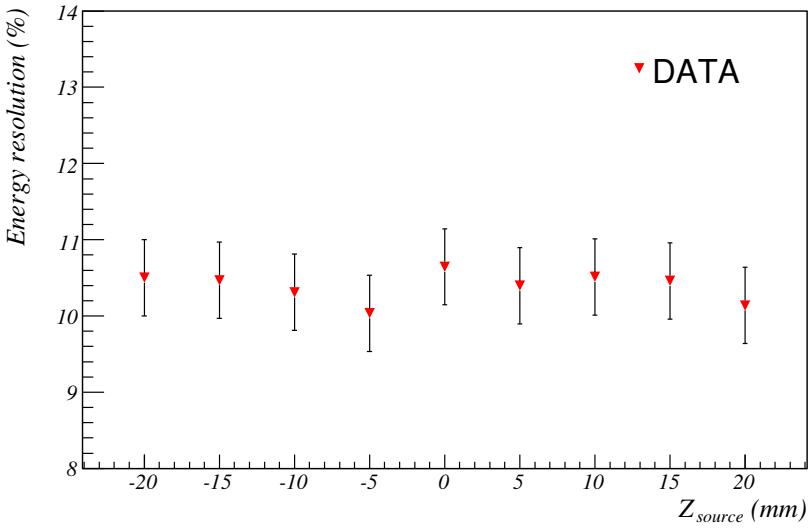

Fig 8. Energy resolution obtained with the two modules scanned by 5 mm steps.

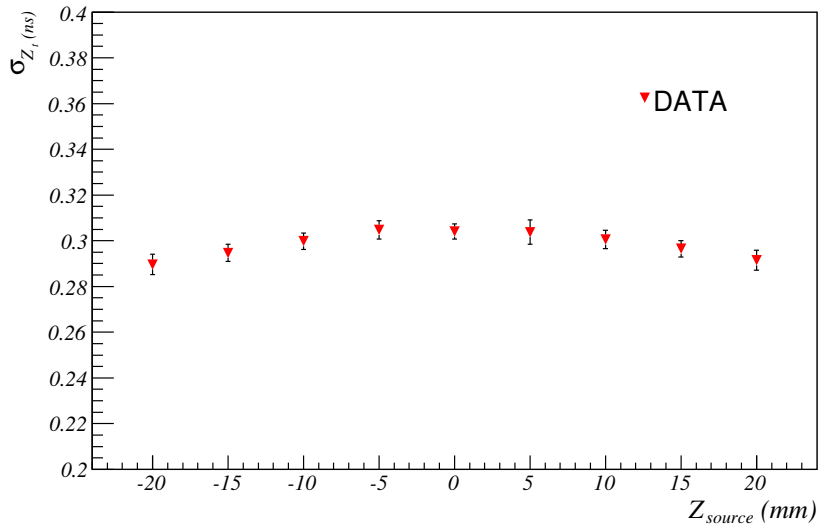

Fig. 9.Time resolution scanned over the two modules by 5 mm steps.

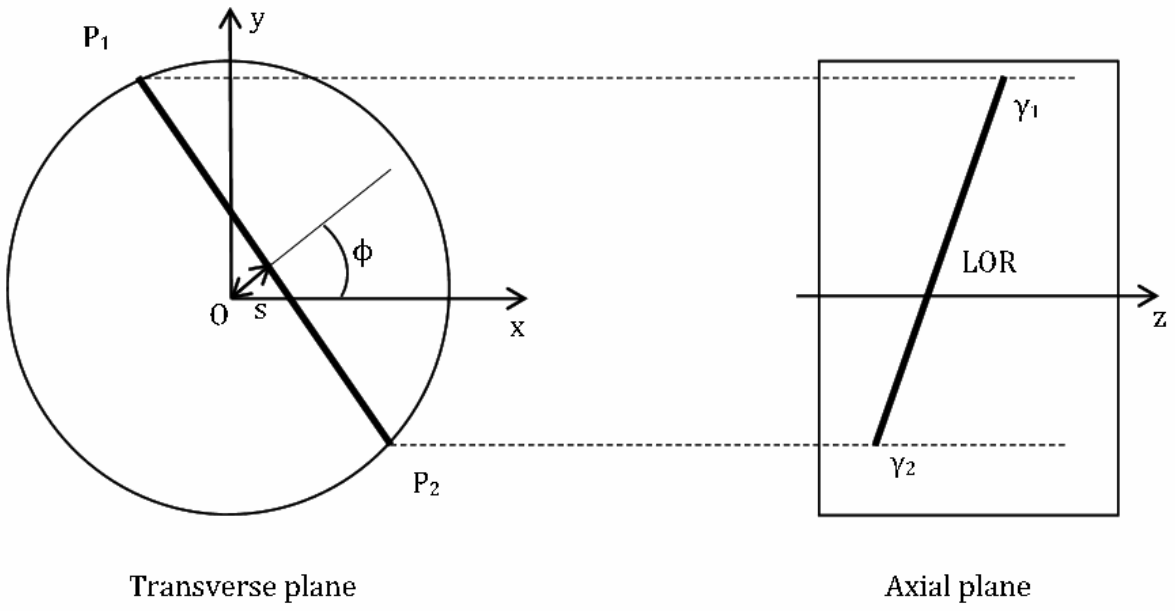

Fig. 10. Definition of the Radon variables (s, ϕ).

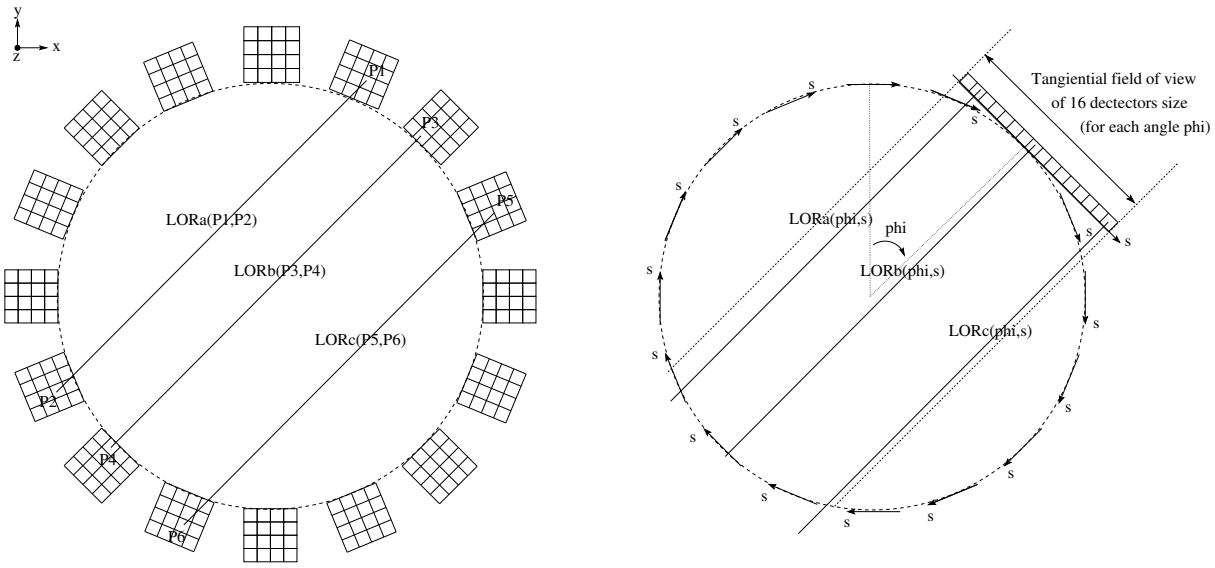

Multi−layer representation of LORs in cartesian space

a LOR is represented by a couple of points P1(x1,y1,z1),P2(x2,y2,z2)

Mono−layer representation of LORs in radon space (s,phi,z)

a LOR is represented by coordinates (s,phi,z)

Fig. 11. Multi-layer and Radon representation of LORs.

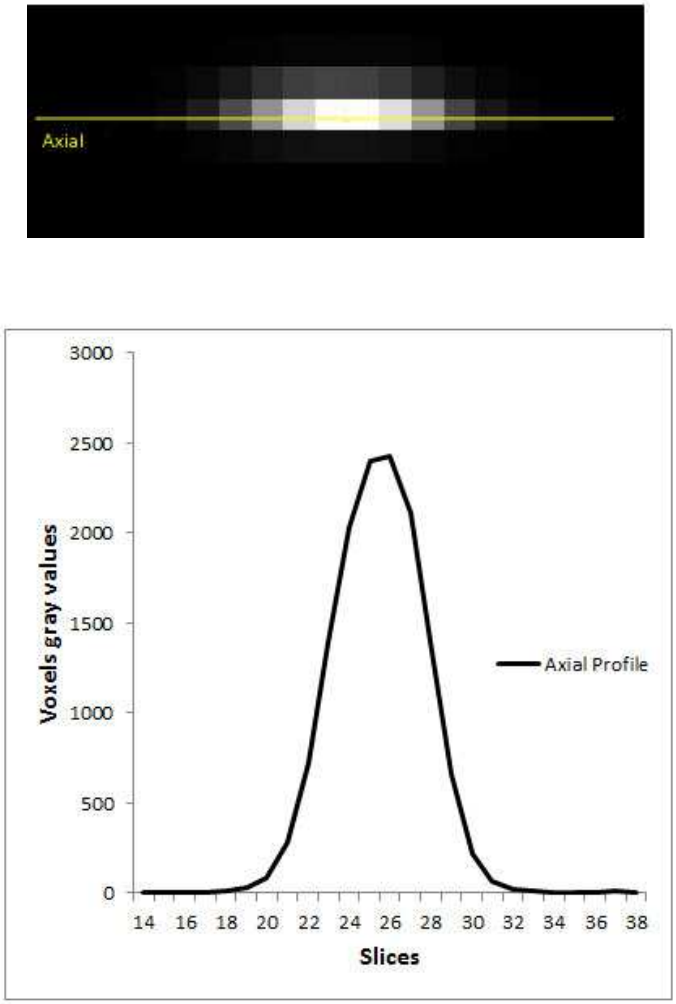

Fig.12. The reconstructed source showed in the axial view (top) and the axial profile (bottom).

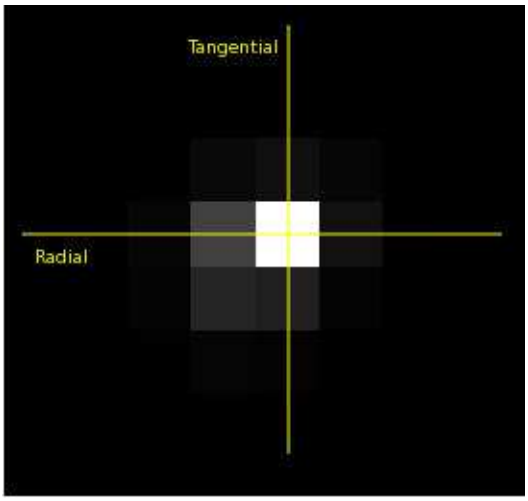

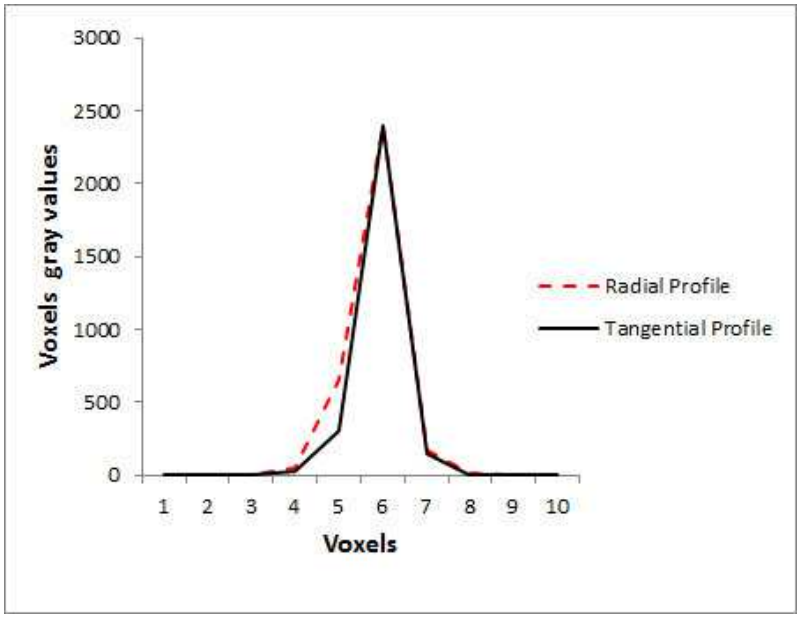

Fig. 13. The reconstructed source shown in the transverse view (top) and the radial and tangential profiles (bottom).

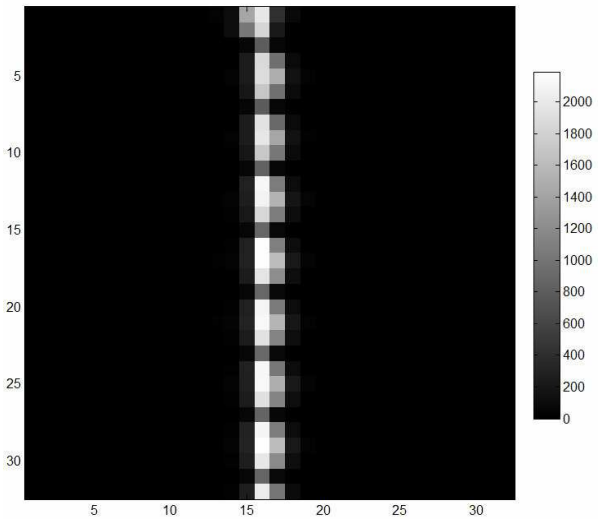

Fig. 14 The central sinogram of the experimental source. The missing data correspond to the lines of low gray level values segmenting the vertical belt of data. Moreover, we notice a shift in the sinogram meaning that the source is slightly off-centered.